SCIENCE CHINA
Information Sciences

• RESEARCH PAPER •

June 2026, Vol. 69, Iss. 6, 162504:1–162504:8
https://doi.org/10.1007/s11432-025-4566-7

Implementation of deterministic quantum spatial searches in a circuit QED system

Qi-Ping SU, Rui-Qi SHEN, Yi-Hao KANG, Lijiong SHEN* & Chui-Ping YANG*

School of Physics, Hangzhou Normal University, Hangzhou 311121, China

Received 19 April 2025/Revised 3 July 2025/Accepted 25 August 2025/Published online 27 April 2026

Abstract Circuit quantum electrodynamics (circuit QED) offers a promising platform for quantum information processing and quantum simulation. The quantum spatial searches for identifying a target vertex on a graph have broad applications across information technologies. However, implementing quantum spatial searches on a graph through circuit QED remains unexplored. In this paper, we propose a scheme to realize quantum spatial searches via continuous-time quantum walks in a circuit QED system. Here, each cavity represents a graph vertex, while a single superconducting (SC) qubit mediates interactions among all cavities, enabling coherent manipulation of the search process in complete graphs. Remarkably, we find that an increasing number of vertices leads to a shorter search time, and the search is achieved deterministically. Our numerical simulations for the target search in an eight-vertex complete graph agree well with theoretical predictions, even under realistic decoherence and experimental parameters. This protocol is universal and can be generalized to accomplish the same task in a wide range of physical systems, where multiple microwave or optical cavities couple to a single matter qubit of various types.

Keywords quantum search, continuous-time quantum walk, circuit QED, complete graph, microwave cavity

Citation Su Q-P, Shen R-Q, Kang Y-H, et al. Implementation of deterministic quantum spatial searches in a circuit QED system. Sci China Inf Sci, 2026, 69(6): 162504, https://doi.org/10.1007/s11432-025-4566-7

1 Introduction

Quantum search techniques play an important role in quantum information processing, which offers a wide range of applications [1–8], such as optimization problems [9], quantum factoring [10], and quantum machine learning [11]. The problem of identifying a target vertex on a graph (i.e., spatial search algorithm) can be effectively modeled using continuous-time quantum walks [12–16]. Spatial searches via continuous-time quantum walks have been explored on graphs with diverse structures [17, 18] and implemented across various quantum systems, including star graphs in linear optics [19] and 2D lattices in neutral atoms [20]. However, a review of the literature reveals that the implementation of continuous-time quantum walk based search algorithms within the framework of circuit quantum electrodynamics (QED) remains unexplored. In particular, the experimental realization of quantum spatial search on complete graphs, where each vertex couples to all others, remains unachieved to date, as it requires high connectivity and presents significant challenges for most quantum platforms.

Circuit QED, which integrates superconducting (SC) qubits with microwave resonators or cavities, has garnered considerable attention due to its exceptional controllability, integrability, ease of fabrication, and potential for scalability [21–30]. Experimental demonstrations have confirmed the strong coupling between SC qubits and microwave cavities [31–33]. Notably, the level spacings of SC qubits can be rapidly tuned within 1–3 ns [34–37], and their coherence time can reach from hundreds of microseconds to over 1 ms [38–44]. Moreover, high-quality microwave cavities, including 1D and 3D configurations, have been experimentally demonstrated with quality factors (photon lifetimes) reaching $Q \gtrsim 2.7 \times 10^6$ (70 μs) and $Q \gtrsim 3.5 \times 10^7$ (2 s), respectively [45–49]. These advancements underscore the potential of circuit QED as a leading platform for quantum computation and quantum simulation [23–27, 50–54].

In this paper, we present (i) the construction of a weighted complete graph (Figure 1(a)) using a circuit QED architecture (Figure 1(b)), and (ii) the implementation of quantum search via continuous-time quantum walks on this platform. The circuit QED system mainly consists of n microwave cavities, which represent n graph vertices. The n cavities simultaneously couple to an SC qubit, enabling interactions between any pair of the cavities. In the search process, an additional SC qubit is utilized to mark the target cavity. We show that the target cavity can

* Corresponding author (email: shenlijiong@hznu.edu.cn, yangcp@hznu.edu.cn)

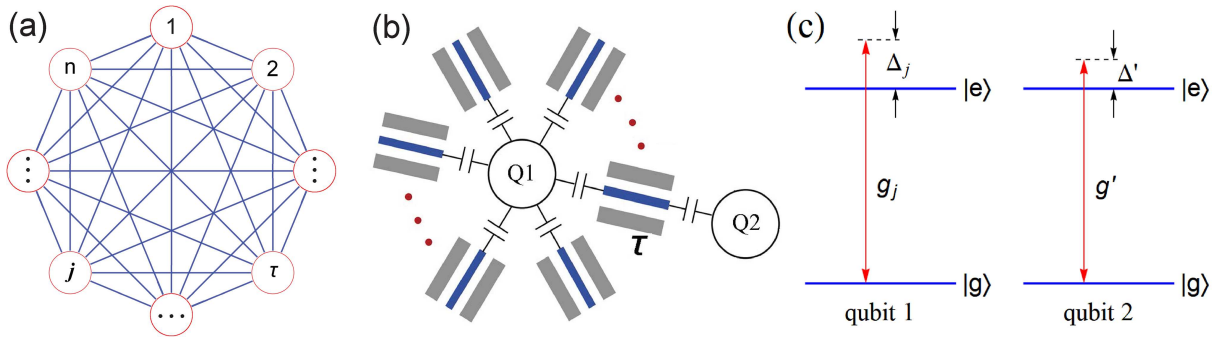

Figure 1 (Color online) (a) Schematic of a complete graph with n vertices, where each vertex is connected to all others. The vertices are depicted as circles, with the target vertex labeled as τ. (b) Setup for constructing a complete graph in circuit QED. All 1D microwave cavities have the same frequency and couple to the SC qubit 1 (denoted as Q1) via capacitors. The target cavity (τ) is marked by its coupling to the SC qubit 2 (denoted as Q2). Note that 1D cavities can be replaced by 3D microwave cavities. (c) Cavity j ($j = 1, 2, \ldots, n$) is dispersively coupled to the $|g\rangle \leftrightarrow |e\rangle$ transition of qubit 1 with coupling constant g_j and detuning Δ_j. Cavity τ is dispersively coupled to the $|g\rangle \leftrightarrow |e\rangle$ transition of qubit 2 with coupling constant g' and detuning Δ'.

be identified with a 100% probability after a short period of free evolution of the system. Numerical simulations, incorporating decoherence, demonstrate that high-fidelity search for a target cavity in an eight-cavity system can be achieved within current circuit QED technology.

This protocol has the following features and advantages. (i) It requires only two auxiliary SC qubits, minimizing hardware resource demands; (ii) the parameters in the search Hamiltonian can be readily adjusted, providing enhanced flexibility; (iii) the search time decreases as the number of graph vertices increases, offering scalability and rapid execution; (iv) the search can be completed in a deterministic way without measurement during the process, thereby ensuring search efficiency; and (v) this protocol is general and can be extended to microwave or optical cavities and single qubits of various types, demonstrating high adaptability.

This paper is organized as follows. In Section 2, we introduce how to implement quantum spatial search in a circuit QED system. In Section 3, we numerically analyze the experimental feasibility of identifying the target in an eight-cavity system. A conclusion is presented in Section 4.

2 Quantum spatial search in circuit QED

We first present an efficient method to construct an n-vertex complete graph (Figure 1(a)) in a circuit QED platform, which consists of n microwave cavities and a SC coupler qubit (i.e., qubit 1 with ground state $|g\rangle$ and excited state $|e\rangle$), as shown in Figure 1(b). Note that qubit 1 does not represent a vertex. To enable interactions between any two cavities, all cavities are coupled to qubit 1 via capacitors. The coupling strength can be adjusted using tunable capacitors [55]. Alternatively, tunable couplers based on superconducting quantum interference devices (SQIDs) can be employed to adjust the coupling strength between the SC qubit and cavities [56, 57]. Moreover, we assume that n microwave cavities have the same frequency ω_c, which can be realized by adopting frequency-adjustable cavities [58, 59].

Then, we use an additional SC qubit (i.e., qubit 2) to couple the target cavity τ, as illustrated in Figure 1(b). Since there does not exist a universal oracle circuit capable of marking the targets, the target elements are usually assumed to be pre-known in the experimental demonstration of quantum search algorithms (e.g., [19, 20, 60–64]). Following the previous studies, we here assume that the search target, i.e., the target cavity, is known.

In the interaction picture and under the rotating-wave approximation (RWA), the Hamiltonian of the system shown in Figure 1(b) is given by ($\hbar = 1$)

$$H = g' a_\tau \left|e\right\rangle_2 \left\langle g\right| \mathrm{e}^{-\mathrm{i}\Delta' t} + \sum_{j=1}^{n} g_j a_j \left|e\right\rangle_1 \left\langle g\right| \mathrm{e}^{-\mathrm{i}\Delta t} + \mathrm{H.C.}, \tag{1}$$

where a_j is the annihilation operator for cavity j, g_j is the coupling constant between cavity j and qubit 1, and $\Delta = \omega_c - \omega_1$ is the detuning between the cavity frequency (ω_c) and the $|g\rangle_1 \leftrightarrow |e\rangle_1$ transition frequency (ω_1) of qubit 1 (Figure 1(c)). Similarly, g' is the coupling constant between the target cavity τ and qubit 2, and $\Delta' = \omega_c - \omega_2$ is the detuning between the cavity frequency (ω_c) and the $|g\rangle_2 \leftrightarrow |e\rangle_2$ transition frequency (ω_2) of qubit 2 (Figure 1(c)).

Under the large detuning conditions $|\Delta| \gg g_j$, $|\Delta'| \gg g'$, and

$$\frac{|\Delta - \Delta'|}{(\Delta)^{-}1 + (\Delta')^{-}1} \gg g'g, \tag{2}$$

we derive the effective Hamiltonian [65]

$$H_{e1} = H_0 + H_I \tag{3}$$

with

$$H_0 = \lambda' \left(a_\tau^\dagger a_\tau \left|g\right\rangle_2 \left\langle g\right| - a_\tau a_\tau^\dagger \left|e\right\rangle_2 \left\langle e\right|\right) + \sum_{j=1}^{n} \lambda_j (a_j^\dagger a_j \left|g\right\rangle_1 \left\langle g\right| - a_j a_j^\dagger \left|e\right\rangle_1 \left\langle e\right|), \tag{4}$$

$$H_I = \sum_{j=1}^{n} \sum_{k=j+1}^{n} \lambda_{jk} (a_j^\dagger a_k + a_j a_k^\dagger)(\left|g\right\rangle_1 \left\langle g\right| - \left|e\right\rangle_1 \left\langle e\right|), \tag{5}$$

where $\lambda' = g'^2/\Delta'$, $\lambda_j = g_j^2/\Delta$, and $\lambda_{jk} = g_j g_k/\Delta$. Note that the interaction term between qubits 1 and 2, mediated through cavity τ, is negligible due to the condition in (2).

Suppose the system is initially in the state $\left|\Psi_0\right\rangle = \left|g\right\rangle_1 \left|g\right\rangle_2 \left|\varphi_0\right\rangle$, with

$$\left|\varphi_0\right\rangle = \frac{1}{\sqrt{n}} \sum_{j=1}^{n} a_j^\dagger \left|00\cdots0\right\rangle. \tag{6}$$

Namely, the two qubits are in their ground states, and the n cavities are in a W state. For example, the W state for three cavities is given by $(a_1^\dagger + a_2^\dagger + a_3^\dagger)\left|000\right\rangle/\sqrt{3} = (\left|100\right\rangle + \left|010\right\rangle + \left|001\right\rangle)/\sqrt{3}$, where $\left|0\right\rangle$ and $\left|1\right\rangle$ denote the vacuum state and the single-photon state of a cavity, respectively. The initial state of the cavities in (6) can be readily prepared by exciting qubit 1 to the state $\left|e\right\rangle$ with a pulse and then allowing it to interact resonantly with the n cavities [66]. The preparation duration t_p is $\pi/2\Omega + \pi/2\sqrt{n}g_r$, where Ω is the Rabi frequency of the pulse and g_r is the coupling strength between each cavity and qubit 1. For example, one has $t_p \simeq 13.5$ ns for $\Omega = g_r = 2\pi \times 25$ MHz and $n = 8$. Note that the system initially contains one photon (i.e., one walker), and the photon number is conserved under the Hamiltonian H_{e1}.

Under the Hamiltonian H_{e1}, the two qubits remain in the ground state $\left|g\right\rangle_1 \left|g\right\rangle_2$ and are not excited. Thus, the effective Hamiltonian H_{e1} simplifies to

$$H_{e2} = \lambda' a_\tau^\dagger a_\tau + \sum_{j=1}^{n} \lambda_j a_j^\dagger a_j + \sum_{j=1}^{n} \sum_{k=j+1}^{n} \lambda_{jk} (a_j^\dagger a_k + a_j a_k^\dagger), \tag{7}$$

which is the effective Hamiltonian governing the dynamics of the cavity system. In a new interaction picture under the Hamiltonian $H_0' = \sum_{j=1}^{n} \lambda_j a_j^\dagger a_j$, the effective Hamiltonian further reduces to

$$H_{e3} = \lambda' a_\tau^\dagger a_\tau + \sum_{j=1}^{n} \sum_{k=j+1}^{n} \lambda_{jk} [a_j^\dagger a_k \mathrm{e}^{\mathrm{i}(\lambda_j - \lambda_k)t} + a_j a_k^\dagger \mathrm{e}^{-\mathrm{i}(\lambda_j - \lambda_k)t}]. \tag{8}$$

Here, the values of the effective coupling strengths λ' and λ_{jk} can be adjusted by changing coupling strengths g_j and g' or detunings Δ and Δ'. The detuning Δ (Δ') can be changed by adjusting the energy-level spacings of SC qubit 1 (2), and the coupling strengths g_j and g' can be adjusted by varying the capacitance between the SC qubits and the cavities.

By adjusting $g_j = g$, $\lambda' = n\lambda$, and $\lambda_j = \lambda_k = \lambda_{jk} = \lambda$, the Hamiltonian in (8) becomes

$$H_e = n\lambda\, a_\tau^\dagger a_\tau + \lambda \sum_{j=1}^{n} \sum_{k=j+1}^{n} [a_j^\dagger a_k + a_j a_k^\dagger]. \tag{9}$$

In the following, we prove that the marked cavity τ can be found under the Hamiltonian H_e. The initial state $\left|\varphi_0\right\rangle$ of the cavities can be expressed as $\left|\varphi_0\right\rangle = \frac{1}{\sqrt{n}}\left|\tau\right\rangle + \frac{\sqrt{n-1}}{\sqrt{n}}\left|s\right\rangle$, where

$$\left|\tau\right\rangle = a_\tau^\dagger \left|00\cdots0\right\rangle \quad \text{and} \quad \left|s\right\rangle = \frac{1}{\sqrt{n-1}} \sum_{j=1(\neq\tau)}^{n} a_j^\dagger \left|00\cdots0\right\rangle. \tag{10}$$

Applying H_e on the states $|\tau\rangle$ and $|s\rangle$, we have

$$H_e|\tau\rangle = n\lambda|\tau\rangle + \lambda\sqrt{n-1}|s\rangle, \quad H_e|s\rangle = \lambda\sqrt{n-1}|\tau\rangle + \lambda(n-2)|s\rangle. \tag{11}$$

Here, we have used

$$\begin{aligned} &n\lambda\ a_\tau^\dagger a_\tau|\tau\rangle = n\lambda|\tau\rangle, \quad \lambda\sum_{j=1}^{n}\sum_{k=j+1}^{n}[a_j^\dagger a_k + a_j a_k^\dagger]|\tau\rangle = \lambda\sqrt{n-1}|s\rangle, \\ &n\lambda\ a_\tau^\dagger a_\tau|s\rangle = 0, \quad \lambda\sum_{j=1}^{n}\sum_{k=j+1}^{n}[a_j^\dagger a_k + a_j a_k^\dagger]|s\rangle = \sqrt{n-1}|\tau\rangle + (n-2)|s\rangle. \end{aligned} \tag{12}$$

Eq. (11) indicates that under H_e, the evolution of the cavity system, starting from the initial state $|\varphi_0\rangle$, remains confined to the two-dimensional subspace spanned by $|\tau\rangle$ and $|s\rangle$.

We now analyze the dynamics of the cavity system within this subspace. The effective Hamiltonian in (9) can be expressed as

$$\begin{aligned} H_e &= (|\tau\rangle\langle\tau| + |s\rangle\langle s|)\cdot H_e\cdot(|\tau\rangle\langle\tau| + |s\rangle\langle s|) \\ &= \lambda\left[n|\tau\rangle\langle\tau| + \sqrt{n-1}|\tau\rangle\langle s| + \sqrt{n-1}|s\rangle\langle\tau| + (n-2)|s\rangle\langle s|\right], \end{aligned} \tag{13}$$

where $\langle\tau|H_e|s\rangle = \langle s|H_e|\tau\rangle = \lambda\sqrt{n-1}$ and $\langle s|H_e|s\rangle = \lambda(n-2)$ have been used. The eigenvalues of this Hamiltonian are $E_\pm = \lambda(n \pm \sqrt{n} - 1)$, with corresponding eigenvectors

$$|\psi_\pm\rangle = \frac{1}{C_\pm}(|\varphi_0\rangle \pm |\tau\rangle), \tag{14}$$

where $C_\pm = \sqrt{2(1 \pm 1/\sqrt{n})}$.

Since the Hamiltonian H_e is time-independent and the initial state can be expressed as $|\varphi_0\rangle = (C_+|\psi_+\rangle + C_-|\psi_-\rangle)/2$ according to (14), the state of the cavity system at time t is given by

$$\begin{aligned} |\varphi(t)\rangle &= \mathrm{e}^{-\mathrm{i}Ht}|\varphi_0\rangle \\ &= \frac{1}{2}(\mathrm{e}^{-\mathrm{i}E_+t}C_+|\psi_+\rangle + \mathrm{e}^{-\mathrm{i}E_-t}C_-|\psi_-\rangle) \\ &= \frac{1}{2}[C_+|\psi_+\rangle + \mathrm{e}^{\mathrm{i}(E_+-E_-)t}C_-|\psi_-\rangle]. \end{aligned} \tag{15}$$

As $|\tau\rangle = (C_+|\psi_+\rangle - C_-|\psi_-\rangle)/2$ from (14), we find that $|\varphi(t)\rangle = |\tau\rangle$ when $(E_+ - E_-)t = \pi$, i.e., $t = \pi/(2\sqrt{n}\lambda)$. This implies that the walker is located at the target vertex with 100% probability at time $\pi/(2\sqrt{n}\lambda)$. In this case, the search time t decreases as either the number of vertices n or the jumping rate λ increases.

From the above description, one can see that the search algorithm based on continuous-time quantum walks is deterministically implemented in the proposed circuit QED system. Notably, the effective coupling strengths between different cavity pairs are adjustable [see H_{e3} in (8)], which enables the construction of weighted graphs and the implementation of other quantum tasks.

3 Experimental feasibility

To demonstrate the feasibility of implementing the search algorithm in circuit QED, we numerically simulate the search process for an eight-vertex graph using eight microwave cavities and two SC transmon qubits. Without loss of generality, we assume that the search target corresponds to cavity 1. Since we assumed that all cavities have the same frequency during the simulation, the calculation results remain the same if the target cavity is set to be any other cavity. In experiments, however, the frequency of each cavity may have a slight difference, and when the target is another cavity, the specific computational results will have slight variations.

Suppose the whole system is initially in the state

$$|\Psi_0\rangle = |g\rangle_1|g\rangle_2\left(\frac{1}{\sqrt{8}}\sum_{j=1}^{8}a_j^\dagger|00\cdots0\rangle\right). \tag{16}$$

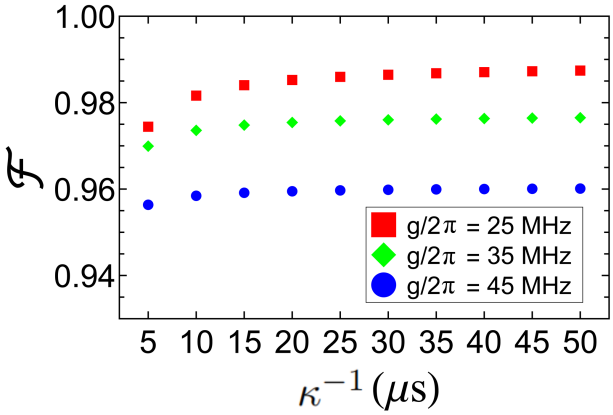

Figure 2 (Color online) Fidelity versus κ^{-1} for coupling strengths $g/2\pi = 25, 35$, and 45 MHz. The numerical simulations are performed with a decoherence time $T = 20$ μs.

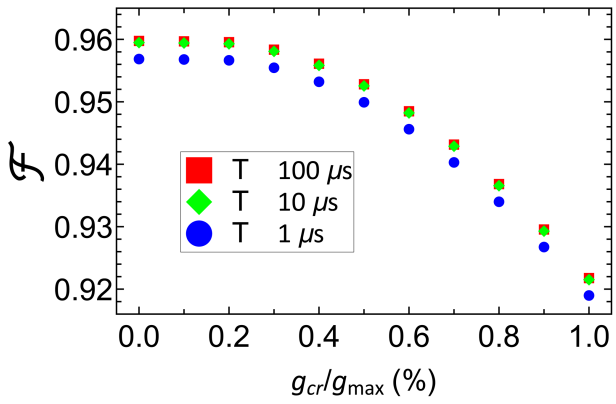

Figure 3 (Color online) Fidelity versus $g_{cr}/g_{\max}$ for decoherence times $T = 100, 10, 1$ μs. Here, g_{cr} denotes the intercavity crosstalk strength, and $g_{\max}$ represents the maximum coupling strength between g and g'. The ratio $g_{cr}/g_{\max}$ varies from 0 to 1%. Numerical simulations are performed with $\kappa^{-1} = 20$ μs and $g/2\pi = 45$ MHz.

To account for dissipation and decoherence in the simulation of the search process, we employ the master equation

$$\frac{d\rho}{dt} = -\mathrm{i}\left[H,\rho\right] + \kappa\sum_{k=1}^{8}\mathcal{L}\left[a_k\right] + \sum_{j=1}^{2}\gamma_{eg}\mathcal{L}\left[\sigma_{eg,j}^{-}\right] + \sum_{j=1}^{2}\gamma_{\phi,e}\left(\sigma_{ee,j}\rho\sigma_{ee,j} - \sigma_{ee,j}\rho/2 - \rho\sigma_{ee,j}/2\right), \tag{17}$$

where $\mathcal{L}\left[\Lambda\right] = \Lambda\rho\Lambda^{\dagger} - \Lambda^{\dagger}\Lambda\rho/2 - \rho\Lambda^{\dagger}\Lambda/2$ (with $\Lambda = a, \sigma_{eg,j}^{-}$), $\sigma_{eg,j}^{-} = \left|g\right\rangle_j\left\langle e\right|$, and $\sigma_{ee,j} = \left|e\right\rangle_j\left\langle e\right|$. In addition, κ is the cavity decay rate, γ_{eg} is the energy relaxation rate for the excited state $\left|e\right\rangle$ of the qubits, and $\gamma_{\phi,e}$ is the dephasing rate for the excited state $\left|e\right\rangle$ of the qubits. Here, H is the Hamiltonian given in (1).

The fidelity is defined as $F = \sqrt{\left\langle\varphi_{id}\right|\rho\left|\varphi_{id}\right\rangle}$, where $\left|\varphi_{id}\right\rangle = \left|g\right\rangle_1\left|g\right\rangle_2\left|10000000\right\rangle$ is the ideal output state, and ρ is the final density matrix obtained by numerically solving the master equation. The parameters used in the numerical simulations are as follows: (i) the detunings are set to $\Delta/2\pi = 1.0$ and $\Delta'/2\pi = 0.125$ GHz; (ii) the relaxation and dephasing rates are $\gamma_{eg}^{-1} = T$ and $\gamma_{\phi,e}^{-1} = T$ [42,43]; (iii) $g' = g$.

We first investigate the effects of the cavity decay time κ^{-1} and the coupling constant g on the fidelity. The results indicate that the influence of κ^{-1} is slight, as shown in Figure 2. This is primarily because the search time is significantly shorter than the values of κ^{-1} used in Figure 2, which are conservative estimates based on current circuit QED experiments [42,43,45,46]. For instance, the search times are approximately 0.045, 0.075, and 0.147 μs for $g/2\pi = 25$, 35, and 45 MHz, respectively. For a fixed detuning Δ, a smaller coupling constant g better satisfies the large detuning condition, which leads to higher fidelity, as demonstrated in Figure 2. The fidelities are approximately 98.5%, 97.5%, and 95.9% for $g/2\pi = 25$, 35, and 45 MHz, respectively.

Next, we investigate the effects of the cavity crosstalk g_{cr} and the decoherence time T of the SC qubits. The crosstalk between cavities can be described by the Hamiltonian

$$H_{cr} = g_{cr}\sum_{j=1}^{8}\sum_{k=j+1}^{8}(a_j^{\dagger}a_k + a_j a_k^{\dagger}), \tag{18}$$

where g_{cr} represents the intercavity crosstalk strength. The ratio of the crosstalk strength g_{cr} to the maximum coupling strength $g_{\max}$ between g and g' can be less than 0.01, as shown in [67,68]. In the following simulations, we use the total Hamiltonian $H + H_{cr}$, with $g/2\pi = g'/2\pi = 35$ MHz and $\kappa^{-1} = 20$ μs. The simulation results are presented in Figure 3, where $g_{\max}$ denotes the maximum coupling strength between g and g'. As expected, the fidelity decreases as g_{cr} increases. For example, the fidelities are about 95.8%, 95.3%, and 92.2% for $g_{cr}/g_{\max} = 0, 0.5\%$, and 1.0%, with $T = 10$ μs. Furthermore, the results indicate that the effect of the qubit decoherence (parameterized by T) is negligible.

4 Conclusion

We have demonstrated the construction of a complete graph using a circuit QED system. We have further demonstrated the implementation of quantum spatial search on the constructed graph through continuous-time quantum walks. Our proposal has several distinguishing features and advantages, as mentioned in the introduction. In particular, an increasing number of vertices can lead to a shorter search time, and the search can be completed deterministically. Our numerical simulations indicate that, in an eight-cavity system, the high-fidelity search can be achieved within current circuit QED technology. To the best of our knowledge, this study is the first to demonstrate the implementation of quantum spatial search on the complete graph constructed in a circuit QED system.

As only basic dispersive coupling between cavities and qubits is required, this proposal is generic and can be applied to accomplish the same task in a wide range of physical systems, where the n cavities can be either microwave or optical cavities and the two auxiliary qubits can be various matter qubits, such as atomic qubits, quantum dots, nitrogen-vacancy centers, magnons, or superconducting qubits with different types. Furthermore, the proposed construction and approach can be extended to implement quantum spatial searches on a variety of graphs, with examples provided in Appendix A.

Acknowledgements This work was supported by National Key Research and Development Program of China (Grant No. 2024YFA1408900), National Natural Science Foundation of China (Grant Nos. U21A20436, 11074062, 11374083, 11774076, 12404404, 12205069, 12204139), Innovation Program for Quantum Science and Technology (Grant No. 2021ZD0301705), Zhejiang Provincial Natural Science Foundation of China (Grant No. LQN25A040019), Hangzhou Leading Youth Innovation and Entrepreneurship Team Project (Grant No. TD2024005), and Hangzhou Normal University Scientific Research and Innovation Team Project (Grant No. TD2025003).

References

1 Giri P R, Korepin V E. A review on quantum search algorithms. Quantum Inf Process, 2017, 16: 315
2 Portugal R. Quantum Walks and Search Algorithms. New York: Springer, 2013
3 Cerezo M, Arrasmith A, Babbush R, et al. Variational quantum algorithms. Nat Rev Phys, 2021, 3: 625–644
4 Montanaro A. Quantum algorithms: an overview. npj Quantum Inf, 2016, 2: 15023
5 He X Y, Sun X M, Zhang J L. Quantum search with prior knowledge. Sci China Inf Sci, 2024, 67: 192503
6 Hong C L, Pei Z, Wang Q D, et al. Quantum attack on RSA by D-wave advantage: a first break of 80-bit RSA. Sci China Inf Sci, 2025, 68: 129501
7 Su J J, Fan J C, Wu S Y, et al. Topology-driven quantum architecture search framework. Sci China Inf Sci, 2025, 68: 180507
8 He X Y, Sun X M, Zhang J L. Quantum search with prior knowledge. Sci China Inf Sci, 2024, 67: 192503
9 Campos R, Casares P A M, Martin-Delgado M A. Quantum metropolis solver: a quantum walks approach to optimization problems. Quantum Mach Intell, 2023, 5: 28
10 Whitlock S, Kieu T D. Quantum factoring algorithm using Grover search. ArXiv:2312.10054
11 Biamonte J, Wittek P, Pancotti N, et al. Quantum machine learning. Nature, 2017, 549: 195–202
12 Childs A M, Goldstone J. Spatial search by quantum walk. Phys Rev A, 2004, 70: 022314
13 Candeloro A, Benedetti C, Genoni M G, et al. Feedback-assisted quantum search by continuous-time quantum walks. Adv Quantum Tech, 2023, 6: 2200093
14 Lugao P, Portugal R, Sabri M, et al. Multimarked spatial search by continuous-time quantum walk. ACM Trans Quantum Comput, 2024, 5: 1
15 Malmi J, Rossi M A C, García-Pérez G, et al. Spatial search by continuous-time quantum walks on renormalized Internet networks. Phys Rev Res, 2022, 4: 043185
16 Apers S, Chakraborty S, Novo L, et al. Quadratic speedup for spatial search by continuous-time quantum walk. Phys Rev Lett, 2022, 129: 160502
17 Peng F, Li M, Sun X. Deterministic discrete-time quantum walk search on complete bipartite graphs. Phys Rev Res, 2024, 6: 033042
18 Wong T G. Grover search with lackadaisical quantum walks. J Phys A, 2015, 48: 435304
19 Qu D, Marsh S, Wang K, et al. Deterministic search on star graphs via quantum walks. Phys Rev Lett, 2022, 128: 050501
20 Young A W, Eckner W J, Schine N, et al. Tweezer-programmable 2D quantum walks in a Hubbard-regime lattice. Science, 2022, 377: 885–889
21 Wallraff A, Schuster D I, Blais A, et al. Strong coupling of a single photon to a superconducting qubit using circuit quantum electrodynamics. Nature, 2004, 431: 162–167
22 Mariantoni M, Wang H, Bialczak R C, et al. Photon shell game in three-resonator circuit quantum electrodynamics. Nature Phys, 2011, 7: 287–293
23 Yang C P, Chu S I, Han S. Possible realization of entanglement, logical gates, and quantum-information transfer with superconducting-quantum-interference-device qubits in cavity QED. Phys Rev A, 2003, 67: 042311
24 Blais A, Huang R S, Wallraff A, et al. Cavity quantum electrodynamics for superconducting electrical circuits: an architecture for quantum computation. Phys Rev A, 2004, 69: 062320
25 You J Q, Nori F. Atomic physics and quantum optics using superconducting circuits. Nature, 2011, 474: 589–597
26 Buluta I, Ashhab S, Nori F. Natural and artificial atoms for quantum computation. Rep Progr Phys, 2011, 74: 104401
27 Xiang Z L, Ashhab S, You J Q, et al. Hybrid quantum circuits: superconducting circuits interacting with other quantum systems. Rev Modern Phys, 2013, 85: 623–653
28 Su Q P, Zhu H H, Yu L, et al. Generating double NOON states of photons in circuit QED. Phys Rev A, 2017, 95: 022339
29 Su Q P, Zhang Y, Bin L, et al. Hybrid controlled-sum gate with one superconducting qutrit and one cat-state qutrit and application in hybrid entangled state preparation. Phys Rev A, 2022, 105: 042434

30 Gu X, Kockum A F, Miranowicz A, et al. Microwave photonics with superconducting quantum circuits. Phys Rep, 2017, 718-719: 1–102
31 Niemczyk T, Deppe F, Huebl H, et al. Circuit quantum electrodynamics in the ultrastrong-coupling regime. Nature Phys, 2010, 6: 772–776
32 Yoshihara F, Fuse T, Ashhab S, et al. Superconducting qubit-oscillator circuit beyond the ultrastrong-coupling regime. Nature Phys, 2017, 13: 44–47
33 Yoshihara F, Fuse T, Ao Z, et al. Inversion of qubit energy levels in qubit-oscillator circuits in the deep-strong-coupling regime. Phys Rev Lett, 2018, 120: 183601
34 Neeley M, Ansmann M, Bialczak R C, et al. Process tomography of quantum memory in a Josephson-phase qubit coupled to a two-level state. Nature Phys, 2008, 4: 523–526
35 Leek P J, Filipp S, Maurer P, et al. Using sideband transitions for two-qubit operations in superconducting circuits. Phys Rev B, 2009, 79: 180511
36 Strand J D, Ware M, Beaudoin F, et al. First-order sideband transitions with flux-driven asymmetric transmon qubits. Phys Rev B, 2013, 87: 220505
37 Barends R, Kelly J, Megrant A, et al. Coherent Josephson qubit suitable for scalable quantum integrated circuits. Phys Rev Lett, 2013, 111: 080502
38 Chang J B, Vissers M R, Córcoles A D, et al. Improved superconducting qubit coherence using titanium nitride. Appl Phys Lett, 2013, 103: 012602
39 Chen Y, Neill C, Roushan P, et al. Qubit architecture with high coherence and fast tunable coupling. Phys Rev Lett, 2014, 113: 220502
40 Stern M, Catelani G, Kubo Y, et al. Flux qubits with long coherence times for hybrid quantum circuits. Phys Rev Lett, 2014, 113: 123601
41 Yan F, Gustavsson S, Kamal A, et al. The flux qubit revisited to enhance coherence and reproducibility. Nat Commun, 2016, 7: 12964
42 Place A P M, Rodgers L V H, Mundada P, et al. New material platform for superconducting transmon qubits with coherence times exceeding 0.3 milliseconds. Nat Commun, 2021, 12: 1779
43 Wang C, Li X, Xu H, et al. Towards practical quantum computers: transmon qubit with a lifetime approaching 0.5 milliseconds. npj Quantum Inf, 2022, 8: 3
44 Somoroff A, Ficheux Q, Mencia R A, et al. Millisecond coherence in a superconducting qubit. Phys Rev Lett, 2023, 130: 267001
45 Woods W, Calusine G, Melville A, et al. Determining interface dielectric losses in superconducting coplanar-waveguide resonators. Phys Rev Appl, 2019, 12: 014012
46 Melville A, Calusine G, Woods W, et al. Comparison of dielectric loss in titanium nitride and aluminum superconducting resonators. Appl Phys Lett, 2020, 117: 124004
47 Reagor M, Pfaff W, Axline C, et al. Quantum memory with millisecond coherence in circuit QED. Phys Rev B, 2016, 94: 014506
48 Kudra M, Biznárová J, Fadavi Roudsari A, et al. High quality three-dimensional aluminum microwave cavities. Appl Phys Lett, 2020, 117: 070601
49 Romanenko A, Pilipenko R, Zorzetti S, et al. Three-dimensional superconducting resonators at $T < 20$ mK with photon lifetimes up to $\tau = 2$ s. Phys Rev Appl, 2020, 13: 034032
50 You J Q, Nori F. Quantum information processing with superconducting qubits in a microwave field. Phys Rev B, 2003, 68: 064509
51 You J Q, Nori F. Superconducting circuits and quantum information. Phys Today, 2005, 58: 42–47
52 Clarke J, Wilhelm F K. Superconducting quantum bits. Nature, 2008, 453: 1031–1042
53 Huang H L, Wu D C, Fan D J, et al. Superconducting quantum computing: a review. Sci China Inf Sci, 2020, 63: 180501
54 Li P B, Liu Y C, Gao S Y, et al. Hybrid quantum device based on NV centers in diamond nanomechanical resonators plus superconducting waveguide cavities. Phys Rev Appl, 2015, 4: 044003
55 Materise N, Dartiailh M C, Strickland W M, et al. Tunable capacitor for superconducting qubits using an InAs/InGaAs heterostructure. Quantum Sci Technol, 2023, 8: 045014
56 Campbell D L, Kamal A, Ranzani L, et al. Modular tunable coupler for superconducting circuits. Phys Rev Appl, 2023, 19: 064043
57 Ye Y, Kline J B, Yen A, et al. Near-ultrastrong nonlinear light-matter coupling in superconducting circuits. Nat Commun, 2025, 16: 3799
58 Kim S, Shrekenhamer D, McElroy K, et al. Tunable superconducting cavity using superconducting quantum interference device metamaterials. Sci Rep, 2019, 9: 4630
59 Bao Z, Wang Z, Wu Y, et al. On-demand storage and retrieval of microwave photons using a superconducting multiresonator quantum Memory. Phys Rev Lett, 2021, 127: 010503
60 Godfrin C, Ferhat A, Ballou R, et al. Operating quantum states in single magnetic molecules: implementation of Grover's quantum algorithm. Phys Rev Lett, 2017, 119: 187702
61 Figgatt C, Maslov D, Landsman K A, et al. Complete 3-Qubit Grover search on a programmable quantum computer. Nat Commun, 2017, 8: 1918
62 Zhang J, Hegde S S, Suter D. Efficient implementation of a quantum algorithm in a single nitrogen-vacancy center of diamond. Phys Rev Lett, 2020, 125: 030501
63 He X, Zhao W T, Lv W C, et al. Experimental demonstration of deterministic quantum search for multiple marked states without adjusting the oracle. Optim Lett, 2023, 48: 4428–4431
64 Li Z H, Yu G F, Wang Y X, et al. Experimental demonstration of deterministic quantum search algorithms on a programmable silicon photonic chip. Sci China-Phys Mech Astron, 2023, 66: 290311
65 James D F, Jerke J. Effective Hamiltonian theory and its applications in quantum information. Can J Phys, 2007, 85: 625–632
66 Ni J H, Zhang D X, Lv W C, et al. Preparation of hybrid W entangled states between superconducting qubits and microwave resonators in circuit QED. Appl Phys Lett, 2024, 125: 17
67 Liu T, Cao X Z, Su Q P, et al. Multi-target-qubit unconventional geometric phase gate in a multi-cavity system. Sci Rep, 2016, 6: 21562
68 Yang C P, Su Q P, Han S. Generation of Greenberger-Horne-Zeilinger entangled states of photons in multiple cavities via a superconducting qutrit or an atom through resonant interaction. Phys Rev A, 2012, 86: 022329

Appendix A Examples of graphs constructed in circuit QED

The configuration in Figure 1(b) of the main text, where one qubit is coupled to multiple cavities, can be generalized to construct other graphs, such as joined complete graphs[1)]. An example of a joined complete graph and its construction in circuit QED are shown in Figures A1(a) and (d), respectively. In our protocol, the size of the searchable database is limited by the number of cavities that can be coupled to a single SC qubit. This limitation arises from the constraints of the chip structure. However, it can be addressed by adopting a joined complete graph structure. For example, the complete graphs within this structure may be distributed across multiple chips.

Furthermore, by resonating the central qubit with cavities, the configuration in Figure 1(b) can be used to realize star graphs [19], such as the 7-vertex graph shown in Figure A1(b) and its realization in Figure A1(e). Note that here the central qubit also represents a vertex. Similarly, complete ternary tree graphs can be constructed, as illustrated in Figures A1(c) and (f). Since only one photon is occupied in the cavities shown in Figure 1(b) (i.e., there is only a single excitation during the search process), the complete graph in Figure 1(a) can also be constructed by replacing the system in Figure 1(b) with n SC qubits simultaneously coupled to a microwave cavity (or a single SC qubit).

After the construction of a graph in circuit QED, the target cavity can be identified after free evolution of the system by marking it via an oracle circuit or an auxiliary qubit. Thus, the configuration in Figure 1(b) is the core of constructing various graphs used for quantum spatial searches. The success probability of finding the target depends on the graph structure. In theory, it reaches 100% in complete graphs [12], approaches 100% in star graphs[2)], but remains considerably below 100% in joined complete graphs[1)].

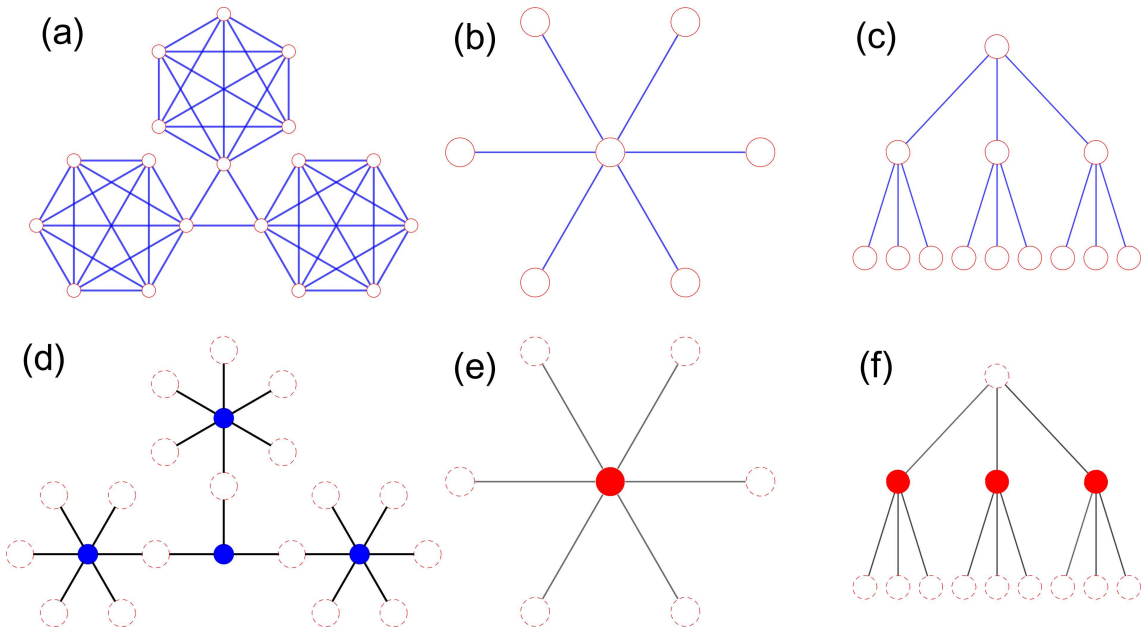

Figure A1 (Color online) Three graph examples constructed using the structure in Figure 1(b) are shown: (a) a joined complete graph formed by three six-vertex complete graphs, (b) a seven-vertex star graph, and (c) a complete ternary tree graph. Vertices and edges are represented by red circles and blue lines, respectively. The corresponding setups in circuit QED for realizing these graphs are illustrated in (d)–(f), with red dashed circles denoting cavities, blue discs denoting SC qubits dispersively coupled to the cavities, while red discs representing SC qubits resonant with the cavities.

1) Meyer D A, Wong T G. Connectivity is a poor indicator of fast quantum search. Phys Rev Lett, 2015, 114: 110503.
2) Cattaneo M, Rossi M A C, Paris M G A, et al. Quantum spatial search on graphs subject to dynamical noise. Phys Rev A, 2018, 98: 052347.